Solid-State Electronics 197 (2022) 108454

Contents lists available at ScienceDirect

Solid State Electronics

journal homepage: www.elsevier.com/locate/sse

# Polarization switching characteristics in AFE/FE Double–Layer devices

Mengqi Fan, Fei Liu, Xiaoyan Liu *

*School of Integrated Circuits, Peking University, Beijing 100871, China*

A B S T R A C T

Ferroelectric/anti-ferroelectric/Ferroelectric(FE/AFE/FE) stack-based multi-bit memory has better device-to-device variation control compared to single-layer FE devices. The interplay between FE and AFE layers hasn't been studied which influences the switching current profile. We simulate the polarization switching characteristics in AFE/FE double layers and analyze their differences from stand-alone devices due to the interplay between the layers. The impacts of spontaneous polarization charges and film thicknesses on the current shift are evaluated, which provides design guidance for these multi-layer devices.

## 1. Introduction

Ferroelectric/anti-ferroelectric/Ferroelectric(FE/AFE/FE) stack-based multi-bit memory has recently been proposed [1], which shows improved device-to-device variation control compared to single-layer FE devices. It benefits from the full switching of the multi-Ec-peaks (intrinsic to anti-ferroelectrics), rather than the partial switching of single-Ec peak of the FE layer, thus reducing the states overlap [1,2]. The current–voltage (IV) characteristics of the stack-based device should meet the following two requirements: (1) To ensure non-volatile storage, switching current of the same polarity should appear at the same voltage side and (2) to reduce states overlap, large separation between these current peaks is favorable [2]. The interplay between FE and AFE layers hasn't been studied which influences the switching current profile. We simulate the polarization switching characteristics in AFE/FE double layers and analyze their differences from stand-alone devices due to the interplay between the layers. The impacts of spontaneous polarization charges and film thicknesses on the current shift are evaluated, which provides design guidance for these multi-layer devices.

## 2. Method and simulated device

Fig. 1 shows the studied double-layer device with FE and AFE thickness of $T_{FE}$ and $T_{AFE}$. The Monte-Carlo based nucleation-limited switching (NLS) [3,4] is used to simulate the polarization switching dynamics. Each layer is assumed to be composed of $N = 500$ independently switching grains. The state $s_{FE}^{(i)}$ of each FE grain $i$ is either $+1(\uparrow)$ or $-1(\downarrow)$, while the state $s_{AFE}^{(i)}$ of AFE grain takes on one of the three states $+1(\uparrow)$, 0, $-1(\downarrow)$, which represents polarized-up, non-polar and polarized-down state respectively. The overall polarization $P_{FE}$ of FE layer is the average of these grains multiplied by the spontaneous polarization charges $Ps_{FE}$.

$$P_{FE} = \frac{Ps_{FE}}{N}\sum_{i=1}^{N} s_{FE}^{(i)} \tag{1}$$

Similarly, for AFE layer, we have:

$$P_{AFE} = \frac{Ps_{AFE}}{N}\sum_{i=1}^{N} s_{AFE}^{(i)} \tag{2}$$

Applying Gauss's Law to the top electrode, the charge density $Q$ on the electrode can be obtained as follows. The *measured* polarization charges in typical polarization–electric field (*P-E*) loops (i.e. charge density on the electrode) also includes the contribution from background dielectric.

For stand-alone devices,

$$Q_{FE(AFE)} = P_{FE(AFE)} + \varepsilon_{FE(AFE)}E \tag{3}$$

For the double layer devices,

$$Q_{double} = \frac{Ps_{AFE}}{N}\sum_{i=1}^{N} s_{AFE}^{(i)} + \frac{\varepsilon_{AFE}}{N}\sum_{i=1}^{N} E_{AFE}^{(i)} \tag{4}$$

where $\varepsilon_{FE}(\varepsilon_{AFE})$ are the permittivity of the FE(AFE) layer; $E$ is the applied electric field of single-layer stand-alone device; $E_{AFE}^{(i)}$ is the electric field in each AFE grain of the double-layer device.

The simulation is time-discretized and for each short time interval $\Delta t$, $s_{AFE}^{(i)}$ and $s_{FE}^{(i)}$ are updated according to the state transition probability $p_{sw}^{(i)}(\Delta t)$, which is described by the Weibull process with history parameter $h_i(t)$ [3,4].

* Corresponding author.
*E-mail address:* xyliu@ime.pku.edu.cn (X. Liu).

https://doi.org/10.1016/j.sse.2022.108454

Available online 15 September 2022

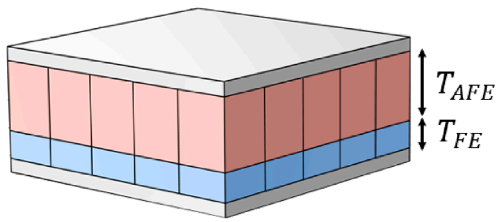


**Fig. 1.** Structure of the AFE/FE double layer device.

**Table 1**
NLS parameters.

| | AFE | FE |
|---|---|---|
| $E_a$ | $2.3 \pm 0.32$ MV/cm | $1.83 \pm 0.43$ MV/cm |
| $E_b$ | $2.1 \pm 0.41$ MV/cm | 0 |
| $\tau_0$ | 73*ns* | 1203 *ns* |
| | Common | |
| $\alpha$ | 4.11 | |
| $n$ | 1.02 | |

$$p_{sw}^{(i)}(\Delta t) = 1 - \exp\{ - [h_i(t+\Delta t)]^n + [h_i(t)]^n \} \tag{5}$$

$$h_i(t+\Delta t) = h_i(t) + \Delta t/\tau_i \tag{6}$$

The time constants $\tau_i$ is a function of the grain electric field $E^{(i)}$ given by [3]:

$$\tau_i(E) = \tau_0 \exp\left[\left(E_a^{(i)}/\left|E^{(i)} - E_b^{(i)}\right|\right)^\alpha\right] \tag{7}$$

where $E_a^{(i)}$ is activation fields and $E_b^{(i)}$ is the backswitching field of each grain, both of which are sampled from Gaussian distributions. The adopted AFE/FE parameters are listed in Table 1. Fig. 2 shows the simulated *P-E* loops and switching currents of the stand-alone devices using parameters from Table-1. The currents are given by the time-derivative of the corresponding polarization charges.

The electrostatics of the dielectric stacks are solved consistently with the NLS models. Charge trapping is not considered in this work.

## 3. Results and discussion

### 3.1. IV characteristics: Three cases

We investigate the switching characteristics in AFE(5 nm)/ FE(2 nm) double-layer device with different spontaneous charges. The applied voltage sweeps from 4.5 V to − 4.5 V and then back. Fig. 3 shows the *P-E* loops (first row) and the corresponding current response (second row) in the three cases, where $Ps_{FE}$ is equal to, smaller or larger than $Ps_{AFE}$. The responses of AFE stand-alone devices are also plotted as reference. In all three cases, the 2nd current peaks shift leftwards, although to a different extent. In Case I, the 1st current peaks on the upward branch barely budge compared to stand-alone AFE devices, while in Case II and Case III, they shift left and right respectively. The responses on the downward branches are symmetrical, so in the following discussion, we will discuss the upward branches only. The shifts of the two switching current peaks with respect to the reference stand-alone AFE capacitor are defined as $\Delta E_{C1}$ and $\Delta E_{C2}$, which are of particular interest to us. We also refer to them as $\Delta E_C$ in the following discussion.

### 3.2. Interplay between the layers

First, we start with a detailed example of Case I with $Ps_{AFE} = Ps_{FE} = 10\mu C/cm^2$. Fig. 4(a) shows the normalized polarization in FE and AFE layer respectively, along with those of the stand-alone devices. Four stages during the upward switching are highlighted. At Stage①, all FE and AFE grains are polarized down and there's no depolarization field. The grains in double layers see the same environment as in the stand-alone devices. Since the AFE grains generally have smaller switching

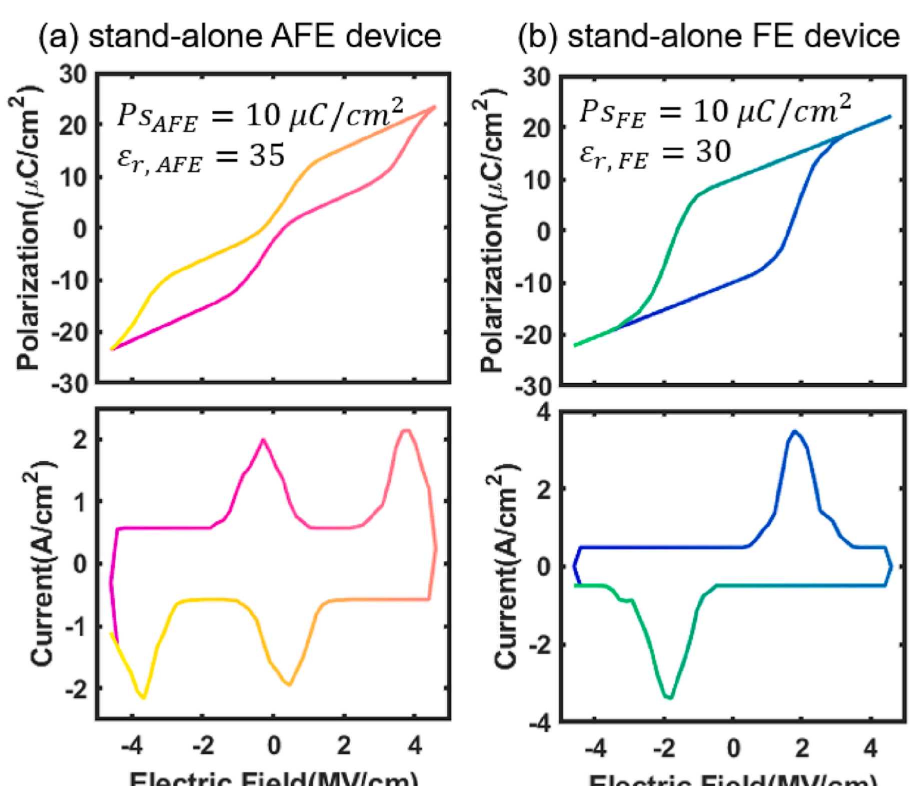


**Fig. 2.** Simulated *P-E* loops and switching current characteristics of single-layer stand-alone: (a) AFE and (b) FE devices using the parameters in table I. $f = 10$ kHz.

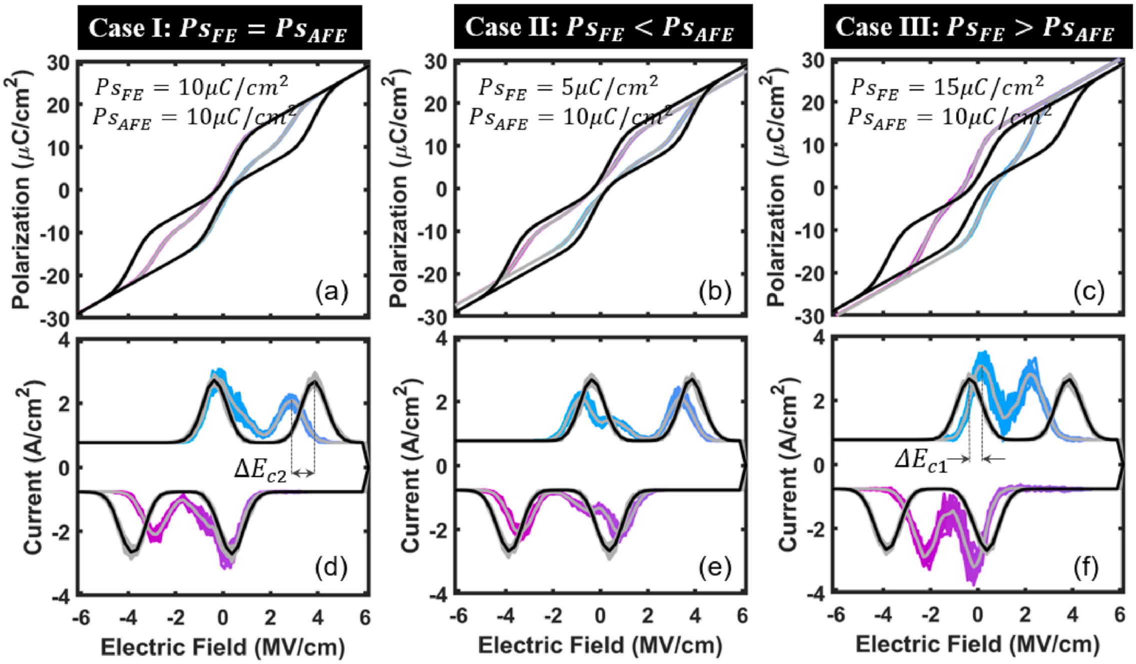


**Fig. 3.** Simulated *P-E* loops (a-c) and switching current (d-f) of the AFE/FE double layers (colored) and the reference stand-alone AFE characteristics (black). $f = 10\,\text{kHz}$. Traces of 20 devices are shown in each case.

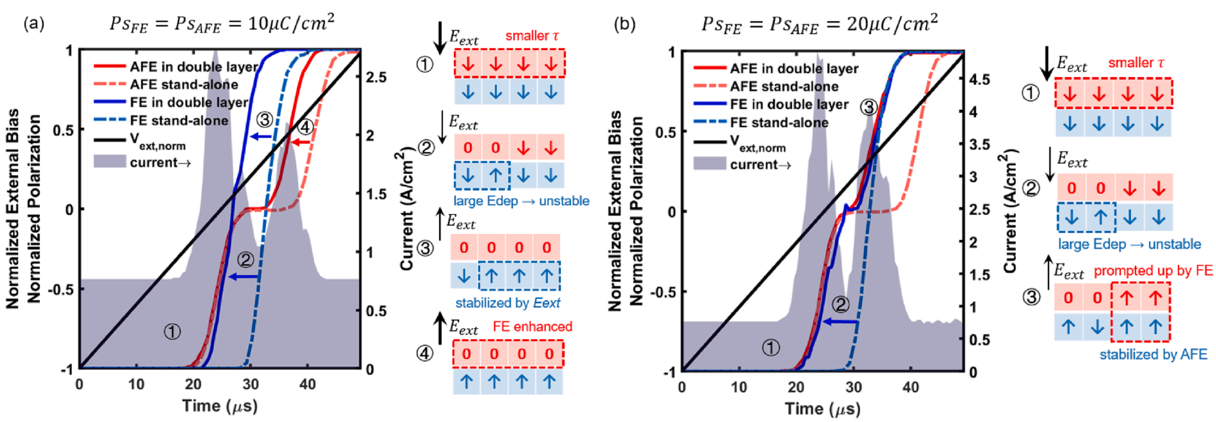


**Fig. 4.** Evolution of normalized polarization in FE and AFE layer in the Case I double-layer device (solid), compared with those in stand-alone devices (dashed). The outline of the shaded area represents the switching current. (a) With small $Ps_{FE}$, AFE switching (stage④) lags behind FE switching (stage③); (b) With large $Ps_{FE}$, FE and AFE polarization switching are closely entwined in Stage ③, resulting in sharper switching current peaks.

time constant τ, AFE switching (from ↓ to 0) occurs earlier than the FE switching. Once the AFE grains switch to zero-state, the polarization charges in the underlying FE grains are not balanced, giving rise to large depolarization field $E_{dep}$. Therefore, in Stage② the depolarization of FE and AFE go hand in hand. Compared with stand-alone FE devices, the $E_{dep}$ accelerates the FE depolarization in the double-layer device. Note that, the depolarization of AFE grain is stable due to the large back-switching barrier $E_b$, whereas the FE grains oscillate between the two polarized states. When the external bias field $E_{ext}$ changes polarity, the increasing $E_{ext}$ helps the FE grains to stay polarized-up in Stage③. In Stage④, the positive polarization charges assist in faster AFE switching.

With larger FE spontaneous polarization charges $Ps_{FE} = 20\mu C/cm^2$, there are some differences in Stage③④ as illustrated in Fig. 4(b). The AFE switching (from 0 to ↑) does not wait until the FE switching stabilized. Instead, the FE polarization charges are sufficiently large to prompt the AFE grains to switch up even when the $E_{ext}$ is weak, which in return stabilizes the FE grains due to charge compensation.

These differences are evidenced in Fig. 5 which shows the grain pattern compositions of the double-layer device and Fig. 5(a) illustrates the transition path of the AFE/FE grain. Initially, when the device is biased at the largest negative point, all the AFE/FE grains are ↓/↓ (light blue). At around 20 μs, the percent of the 0/↓ and 0/↑ grain patterns (dark blue and tangerine) gradually increase as the ↓/↓ patterns decreases. The two dashed lines for Ps = 20 μC/cm$^2$ are overlapped indicating, as mentioned before, that the FE grains are not stable when the external bias is weak. For the case of Ps = 10 μC/cm$^2$, there's a moment (around 30 μs) when the 0/↑ grains account for more than 95 % of the AFE/FE grains. In contrast, for the case of $Ps = 20\mu C/cm^2$, the premature ending of the increase of 0/↑ grains agrees with the early onset of ↑/↑ grains (yellow).

The FE and AFE polarization switching are closely entwined in Fig. 4 (b) and hence the switching current peaks are sharper than those in Fig. 4(a). On the other hand, if $Ps_{FE}$ is very small, its $E_{dep}$ is not large enough and the FE depolarization current might be separated from the AFE depolarization current (i.e. 1st current peak) as shown by the hump in Fig. 3(e).

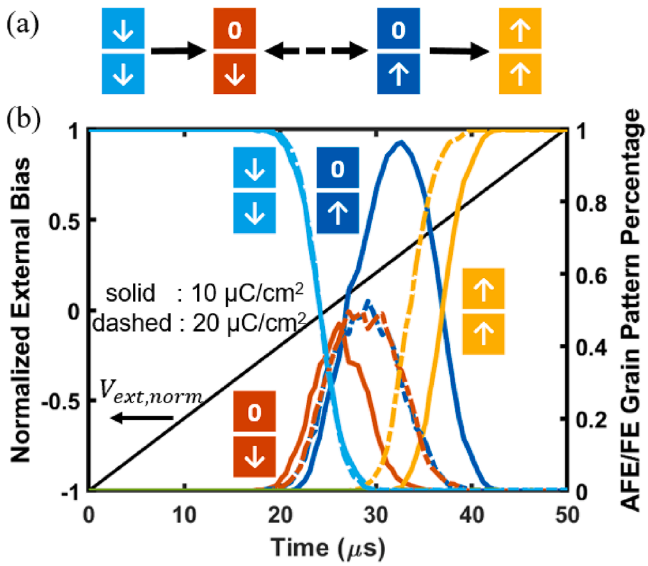


**Fig. 5.** (a) The transition path of the polarization pattern for AFE/FE grain. (b) The composition evolution of AFE/FE grain patterns for devices with $Ps_{FE} = Ps_{AFE} = 10\mu C/cm^2$ (solid) and $Ps_{FE} = Ps_{AFE} = 20\mu C/cm^2$ (dashed).

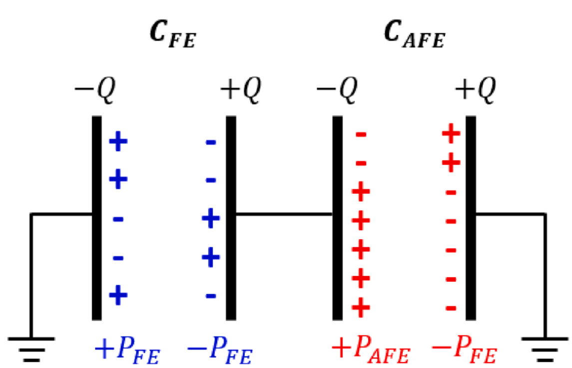


**Fig. 6.** The AFE/FE double-layer device is modelled as two capacitor connected in series in the calculation.

As for Case II, the main difference from Case I lies in Stage①, where the under-compensation of the AFE polarization charges, leads to the expedited AFE switching compared with stand-alone AFE devices, thus the first switching current peak shifts left. Conversely, in Case III, the AFE switching is delayed.

### 3.3. Design guidance

Compared with the reference stand-alone AFE devices, the current shift $\Delta E_C$ of the double-layer device arises from the polarization charge mismatch between the two layers (i.e. $P_{FE} \neq P_{AFE}$), which leads to the depolarization field or the enhancement field over the AFE layer.

To estimate $\Delta E_C$, the AFE/FE double-layer device is modelled as two capacitor connected in series [5] as schematically shown in Fig. 6. When no external bias is applied, the voltage drop over the FE and AFE layer, denoted by $V_{FE}$ and $V_{AFE}$ respectively, are determined by: (1) the overall polarization charges $P_{FE}$ and $P_{AFE}$; (2) the induced charges on the electrode Q.

$$V_{FE} = \frac{Q - P_{FE}}{C_{FE}} \tag{8a}$$

$$V_{AFE} = \frac{Q - P_{AFE}}{C_{AFE}} \tag{8b}$$

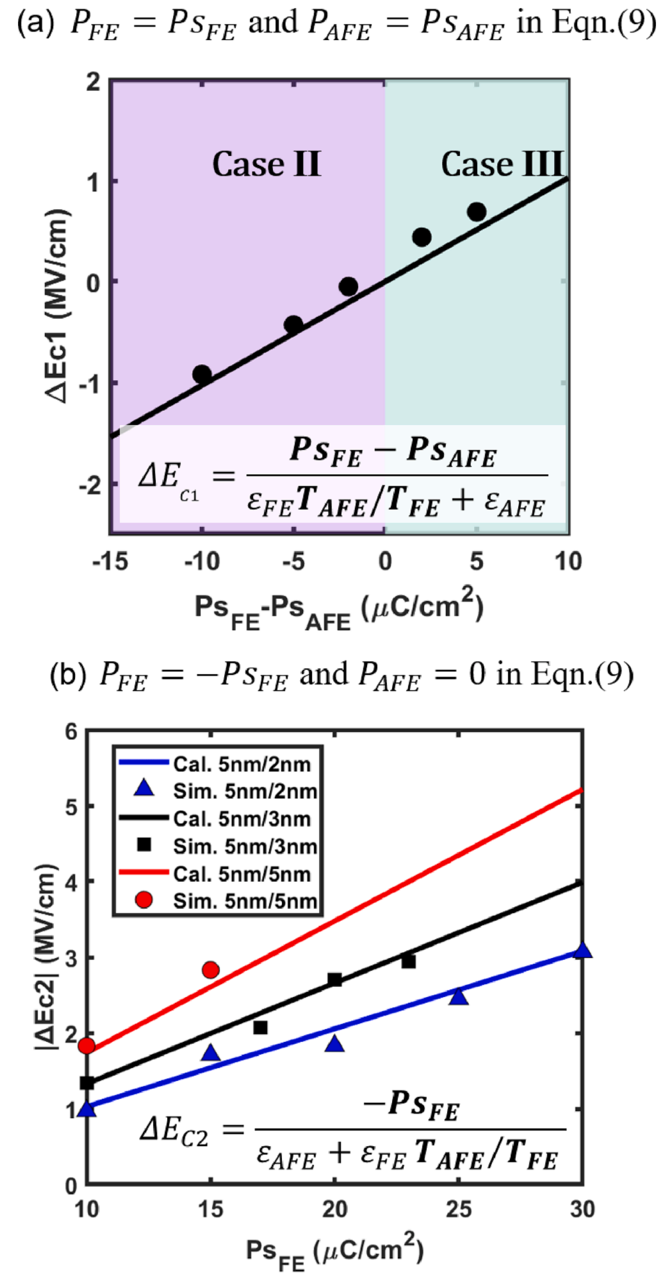


**Fig. 7.** (a) The linear dependence of 1st current peak shift $\Delta E_{C1}$ on $Ps_{FE} - Ps_{AFE}$. (b) The linear dependence of 2nd current peak shift $\Delta E_{C2}$ on $Ps_{FE}$. Increase thickness ratio $T_{AFE}/T_{FE}$ results in increase $\Delta E_{C2}$.

$$V_{FE} + V_{AFE} = 0 \tag{8c}$$

where $C_{FE}$ and $C_{AFE}$ are their capacitance. By eliminating $Q$, we have:

$$\Delta E_C = \frac{V_{AFE}}{T_{AFE}} = \frac{P_{FE} - P_{AFE}}{\varepsilon_{FE} T_{AFE}/T_{FE} + \varepsilon_{AFE}} \tag{9}$$

Then we only need to find out the $P_{FE}$ and $P_{AFE}$ right before each AFE switching peak, while the detailed switching dynamics are omitted. According to Fig. 4 and Fig. 5, before the 1st switching peak (stage①), both FE and AFE grains are polarized down. Therefore, for $\Delta E_{C1}$, $P_{FE} = Ps_{FE}$ and $P_{AFE} = Ps_{AFE}$. Before the 2nd switching peak (stage③), the AFE grains are depolarized and the FE grains have been switched up, more or less. Therefore, for $\Delta E_{C2}$, $P_{FE} = -Ps_{FE}$ and $P_{AFE} = 0$.

As shown in Fig. 7, the results calculated with Eq. (9) agree well with the simulated results. The slope of both $\Delta E_{C1}(\propto Ps_{FE} - Ps_{AFE})$ and

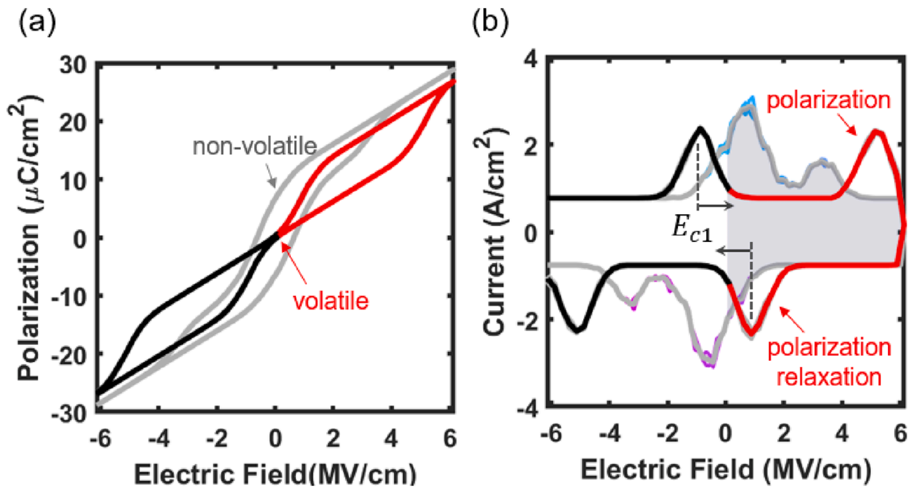


**Fig. 8.** Simulated (a) *P-E* loops and (b) *I-V* curves of non-volatile AFE(4 nm)/FE(3 nm) double-layer device (grey line) as well as the reference stand-alone AFE capacitor. For sake of illustration, some of the NLS parameters ($E_a$ = 2.8 ± 0.32 MV/cm, $E_b$=3.0 ± 0.41 MV/cm for AFE and$E_a$ = 3.2 ± 0.43 MV/cm for FE) are modified to show a completely pinched AFE *P-E* loop.

$\Delta E_{C2}(\propto Ps_{FE})$ increase with decreasing thickness ratio $T_{AFE}/T_{FE}$.

To ensure non-volatility of the multi-layer device, $E_{C1}$ is expected to be positive. Namely, $\Delta E_{C1}$ should be large enough. Fig. 8 illustrate the non-volatility requirement. Note that, for AFE capacitor, there are two switching current peaks of opposite polarity on the right half-plane and consequently the remnant polarization is zero. By contrast, the double-layer device, with $E_{C1} > 0$, exhibits current peaks of the same polarity and thus shows non-zero remnant polarization. However, by increasing $Ps_{FE}$ or decreasing $T_{AFE}/T_{FE}$, $|\Delta E_{C2}|$ also increases with $\Delta E_{C1}$ and consequently risks merging of the two *Ec* peaks. Since the multi-*Ec*-peaks is the prerequisite of the superior device-to-device variation in these stack-based devices, this implies a trade-off between the non-volatility and small variation. Alternatively, by decreasing $Ps_{AFE}$, $\Delta E_{C1}$ increase does not affect $\Delta E_{C2}$ but reduce the remanent polarization.

## 4. Conclusion

We investigate the switching characteristics of AFE/FE double layer devices using NLS model. It is found that AFE and FE switching are more closely coupled in devices with larger $Ps_{FE}$. The switching current shifts and their dependences on spontaneous polarization and film thicknesses are given, which may serve as guidance for device design.

## Declaration of Competing Interest

The authors declare that they have no known competing financial interests or personal relationships that could have appeared to influence the work reported in this paper.

## Data availability

The authors are unable or have chosen not to specify which data has been used.

## References

[1] Y. Xu, *et al.*, “Improved Multi-bit Storage Reliablity by Design of Ferroelectric Modulated Anti-ferroelectric Memory,” 2021 IEEE International Electron Devices Meeting (IEDM). pp.126-129.
[2] K. Ni et al., “A novel ferroelectric superlattice based multi-level cell non-volatile memory,” in 2019 IEEE International Electron Devices Meeting (IEDM). pp. 28.8. 1-28.8.4.
[3] Y.-C. Chen *et al.*, “NLS based Modeling and Characterization of Switching Dynamics for Antiferroelectric / Ferroelectric Hafnium Zirconium Oxides,” 2021 IEEE International Electron Devices Meeting (IEDM). pp. 338-341.
[4] C. Alessandri, *et al.*, “Experimentally Validated, Predictive Monte Carlo Modeling of Ferroelectric Dynamics and Variability,” 2018 IEEE International Electron Devices Meeting (IEDM). pp. 368-371.
[5] Ma TP, et al. Why is nonvolatile ferroelectric memory field-effect transistor still elusive? IEEE Electron Device Lett 2002;23(7):386–8.